JACS
JOURNAL OF THE AMERICAN CHEMICAL SOCIETY
Article
Cite This: J. Am. Chem. Soc. 2018, 140, 14789−14798
pubs.acs.org/JACS

Direct Observation of Murine Prion Protein Replication in Vitro

Jason C. Sang,[†] Georg Meisl,[†] Alana M. Thackray,[‡] Liu Hong,[†,§] Aleks Ponjavic,[†] Tuomas P. J. Knowles,[†,#] Raymond Bujdoso,[‡] and David Klenerman*[,†]

[†]Department of Chemistry, University of Cambridge, Cambridge, CB2 1EW, U.K.
[‡]Department of Veterinary Medicine, University of Cambridge, Cambridge, CB3 0ES, U.K.
[§]Zhou Pei-Yuan Center for Applied Mathematics, Tsinghua University, Beijing 100084, PR China
[#]Cavendish Laboratory, University of Cambridge, Cambridge, CB3 0HE, U.K.

Supporting Information

ABSTRACT: Prions are believed to propagate when an assembly of prion protein (PrP) enters a cell and replicates to produce two or more fibrils, leading to an exponential increase in PrP aggregate number with time. However, the molecular basis of this process has not yet been established in detail. Here, we use single-aggregate imaging to study fibril fragmentation and elongation of individual murine PrP aggregates from seeded aggregation in vitro. We found that PrP elongation occurs via a structural conversion from a PK-sensitive to PK-resistant conformer. Fibril fragmentation was found to be length-dependent and resulted in the formation of PK-sensitive fragments. Measurement of the rate constants for these processes also allowed us to predict a simple spreading model for aggregate propagation through the brain, assuming that doubling of the aggregate number is rate-limiting. In contrast, while α-synuclein aggregated by the same mechanism, it showed significantly slower elongation and fragmentation rate constants than PrP, leading to much slower replication rate. Overall, our study shows that fibril elongation with fragmentation are key molecular processes in PrP and α-synuclein aggregate replication, an important concept in prion biology, and also establishes a simple framework to start to determine the main factors that control the rate of prion and prion-like spreading in animals.

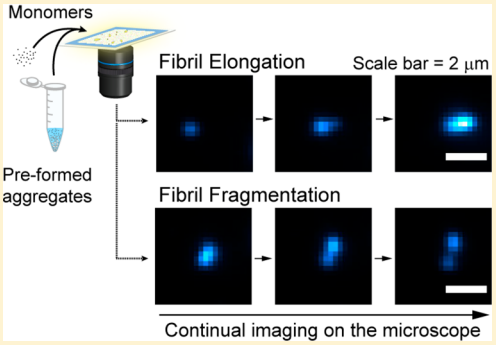

INTRODUCTION

Prion diseases are fatal neurodegenerative conditions of various vertebrate species, characterized by conversion of the normal form of the predominantly α-helical host protein PrP^{C}, into the β-sheet-enriched abnormal conformer PrP^{Sc}. According to the prion hypothesis, the transmissible prion agent comprises principally PrP^{Sc}.[1] Several lines of experimental evidence have collectively provided strong support for the prion hypothesis. These include the generation of PrP transgenic mice that develop spontaneous neurodegenerative disease that is transmissible[2−4] and in vitro generation of infectious prions.[5,6] Prion diseases are an important model for protein misfolding neurodegenerative conditions in general, since several of these diseases, including Alzheimer's disease (AD) and Parkinson's disease (PD), show features of prion-like transmission in experimental settings, evidenced by transcellular spread of misfolded disease-specific protein.[7,8] While the injection of α-synuclein fibrils has been shown to lead to prion-like spreading in animal models of PD,[9] there is currently no quantitative framework to extrapolate these results to humans, and hence it remains to be established if prion-like spreading occurs in PD.

Prion replication occurs by a nucleation-dependent polymerization reaction, whereby growth of aggregated PrP nuclei is followed by fast elongation through recruitment of misfolded PrP monomers to the protein assemblies.[10] Several molecular events are proposed to play a key role in this process, such as fibril fragmentation[11−13] (Figure 1a). Fibril fragmentation increases the number of protein assemblies by generating multiple fragments, and thus providing new ends for monomer addition, a process that becomes important in the later stage of assembly aggregation.[13] Fibril fragmentation has been demonstrated to accelerate prion replication in yeast prion Sup35[11,14] and Ure2,[15] as well as α-synuclein (αS) in PD,[16] while few insights have been provided from mammalian prion studies.[17] Significantly, there is no clear evidence that mammalian prions show a similar phenomenon of fragmentation during aggregation. Therefore, it is important to determine the mechanism and kinetics of how PrP aggregates grow and amplify, since these events will provide fundamental insights into how prions might spread in the brains of individuals affected by prion diseases.

Dissecting the mechanism of prion propagation in vivo is difficult given the molecular and cellular complexity of the mammalian brain. As a consequence, this process has been increasingly studied with recombinant prion protein in vitro. Compared with conventional biochemical and biophysical approaches, single-molecule fluorescence microscopy serves as

Received: August 3, 2018
Published: October 10, 2018

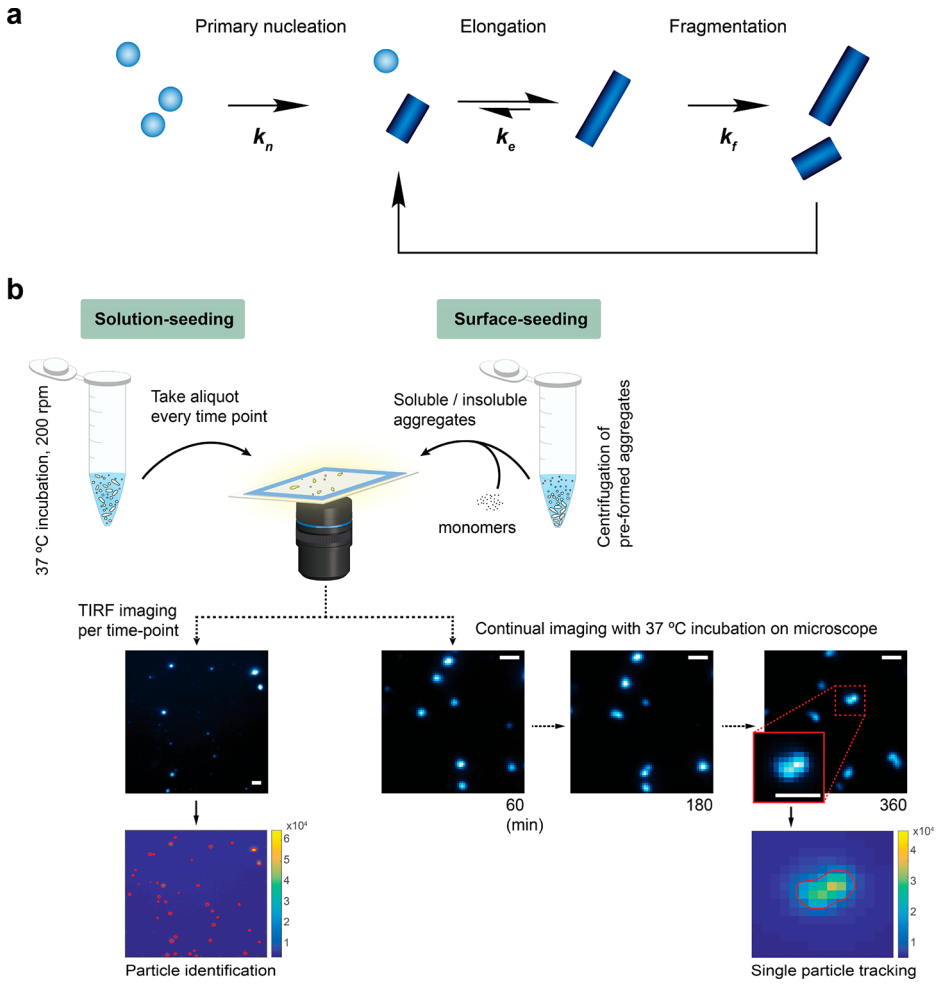

Figure 1. Schematic description of the molecular processes of fibril formation and the experimental setup. (a) Amyloid fibril formation begins with slow primary nucleation that involves a range of structurally diverse intermediates, followed by fast growth of fibrils. The fibrils can break into smaller fragments and act as new templates for further growth. (b) In the bulk solution-seeded measurements (left), PrP aggregates were incubated in a 1.5 mL centrifuge tube. At various time points, aliquots were removed from the reaction mix and transferred to a solution containing ThT, and the aggregates subsequently diluted to a nanomolar concentration. The PrP aggregates were imaged on a TIRF microscope with a 3 × 3 image grid at 3 random positions (i.e., 27 simultaneous images). The acquired images were analyzed with a Matlab-based script to identify individual aggregates (see Experimental Procedures in the Supporting Information for details). For the surface-seeded measurements (right), preformed soluble or insoluble seeds were separated by centrifugation and then adsorbed onto a glass coverslip. After removal of residual solution, fresh PrP monomers and ThT were added to the glass coverslip and slide chamber sealed to prevent fluid evaporation. Images of individual aggregates were acquired over time in a single 3 × 3 image grid with fixed fields of view at 37 °C (i.e., 9 simultaneous images). All the scale bars represent 2 μm.

a powerful tool by resolving the behavior of individual protein aggregates that may be averaged in ensemble experiments. Recently, we have developed "single-aggregate" fluorescence imaging to visualize protein aggregates through the use of sensitive total internal reflection fluorescence (TIRF) microscopy in combination with thioflavin T (ThT).[18] This method provides direct observation of the low-populated species such as oligomers, which are naturally heterogeneous, transient, and metastable during aggregation.[16,19−22] It also enables us to quantitatively measure the change in the number of individual aggregates as a function of time. Furthermore, as ThT molecules bind and unbind from the protein aggregates in equilibrium, this approach allows protein assemblies to be imaged for extended time periods without photobleaching and for biochemical assays, such as proteinase K (PK) resistance measurements, to be performed on individual aggregates.

Here, we have adapted the single-aggregate fluorescence imaging to visualize the aggregation process of recombinant PrP and αS under native conditions. In this present study, we have quantitatively measured PrP and αS aggregation in vitro as a function of time. This has allowed us to determine, for the first time to our knowledge, the elongation and fragmentation rate constants for PrP aggregation through the use of a kinetic modeling approach. These parameters thus enabled us to predict the spread of PrP through the brain based on a simple model. We also show that αS replication is likely to follow the same elongation−fragmentation mechanism with a significantly slower elongation and fragmentation rate than PrP. In addition, we find that during the aggregation reaction, both PrP and αS convert from a PK-sensitive to PK-resistant conformer. The fragmentation rate increases with fibril length, and this process results in the formation of PK-sensitive fragments. This study demonstrates our ability to quantitatively compare the prion-like properties between PrP and αS, and reveals the key role of fibril fragmentation and elongation in prion and prion-like replication.

DOI: 10.1021/jacs.8b08311
J. Am. Chem. Soc. 2018, 140, 14789−14798

RESULTS

Kinetic Rate Constants of PrP Aggregation Can Be Determined from Solution-Seeded Reactions under Native Conditions. Kinetic rate constants for the elongation and fragmentation process of amyloidogenic proteins can be derived from quantitative measurements during aggregation.[23] To acquire the kinetic parameters for PrP aggregation, we performed a set of seeded reactions of murine recombinant PrP in bulk solution under native conditions (Figure 1b, left).

To produce seeds, PrP aggregates were generated following a previously published protocol.[24] Small aggregates (Figure S1a,b), as well as large fibrils (Figure S1c), were obtained after 48 h, when the reaction reached a plateau. The aggregate mixture was then separated by centrifugation to obtain soluble aggregates from the supernatant (soluble seeds), or insoluble aggregates (insoluble seeds; acquired from sonication of the fibrillary species after pellet resuspension). Prior to imaging PrP seeds, we established optimal conditions where the number of PrP aggregates adsorbed onto a glass surface was proportional to their solution concentration (Figure S2), which means the surface was not saturated by the aggregates.

Next, we carried out PrP aggregation using the soluble seed in the reaction buffer (50 mM sodium phosphate buffer, pH 7.0) with a wide range of seed and monomer concentrations. At defined time points during the seeded aggregation reaction, aliquots were removed from the reaction mix, and the number of PrP aggregates present quantified using ThT and TIRF microscopy (Figure 1b, left). Seeded PrP aggregation was found to proceed through exponential amplification, as shown in Figure 2. We found that gentle shaking of the reaction mix was required in order for PrP to form aggregates. This is consistent with conditions used for QuIC experiments[25] and was possibly due to a fraction of the aggregates adsorbed on the microcentrifuge tube surface. Interestingly, we also observed fast disappearance of PrP aggregates after the reaction reached a plateau. Through the use of transmission electron microscopy (TEM), we observed that the PrP aggregates that disappeared in TIRF images were ThT-inactive and small fragments (<50 nm) (Figure S3) that probably formed due to fragmentation.

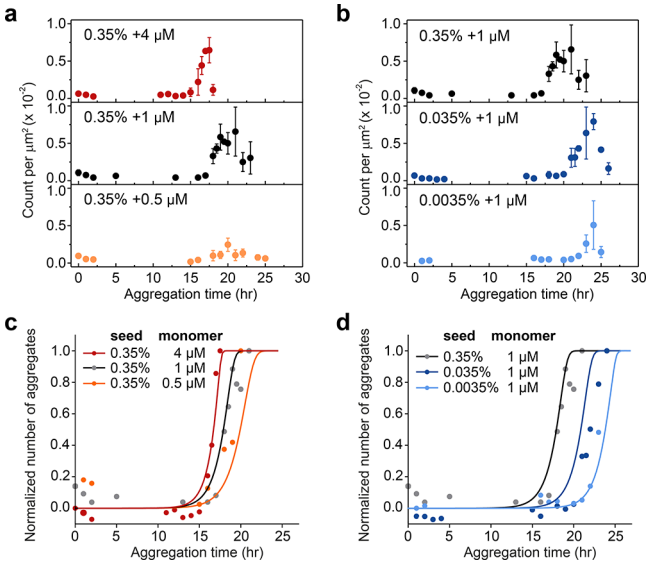

Figure 2. Kinetics of solution-seeded PrP aggregation in 50 mM sodium phosphate (pH 7.0). (a,b) The kinetics were measured by taking aliquots at various time points from aggregation reaction mix that was incubated at 37 °C with shaking at 200 rpm. (c,d) Fits of the kinetic profiles. The *y*-axis was normalized to the maximum value of each profile. The product of the rate constants, $k_e k_f$, for solution-seeded PrP aggregation was 0.06 ± 0.03 M^{-1} s^{-2}. The error bars represent standard deviations from three independent experiments.

To acquire kinetic parameters for PrP aggregation, the data was globally fitted to a kinetic model for protein aggregation that we have published previously.[12,26] This model has two parameters: the elongation rate constant, k_e, and the fragmentation rate constant, k_f. When we consider the time required for a single misfolded PrP aggregate elongate and fragment to form two aggregates, the doubling time t_2, is given by

$$t_2 = \frac{\ln 2}{\sqrt{(2k_e k_f m)}} \quad (1)$$

where m is the monomer concentration (see Experimental Procedures in the Supporting Information for details). From the global fit to the solution-seeded data (Figure 2c), the product of k_e and k_f was found to be 0.06 M^{-1} s^{-2} (Table 1).

According to eq 1, the doubling time t_2 for PrP amplification in a cell depends on the rate constants, k_e and k_f, as well as subcellular PrP^C concentration (m) at the cellular location where PrP^C-PrP^{Sc} conversion takes place. Since this conversion site in cells is still debated,[27−30] we assumed that PrP aggregation occurs at the plasma membrane and the corresponding local PrP^C concentration is 60 nM (see Supporting Information for details). Using the rate constants obtained from the solution-seeded reaction with soluble seeds, t_2 was estimated to be 2.2 h for PrP assembly propagation on the plasma membrane. In comparison, if PrP aggregation is assumed to take place in the endosomal compartments, where the local PrP^C concentration is 15 nM, the estimated t_2 would slightly increase to 4.4 h, showing that t_2 is not very sensitive to the monomer concentration (Table 1).

PrP Fragmentation and Elongation Are Directly Observed from Surface-Seeded Aggregation. Next, to study the fragmentation kinetics of PrP, we performed surface-seeded aggregation reactions under the same native conditions as above, which allowed continual measurements of fixed fields of view on a coverslip surface. Experiments were achieved by adsorbing either the soluble or insoluble seed onto a glass coverslip, removing the residual solution, followed by the addition of PrP monomers into the reaction mix. Changes in the morphology and the size of individual PrP aggregates were visualized over time by continual imaging of the same fields of view on a microscope stage at 37 °C (Figure 1b, right). We followed more than 10 000 aggregates during surface-seeded aggregation reactions using the soluble or insoluble seeds, respectively. Interestingly, 8.7% (soluble) and 4.4% (insoluble) of the PrP aggregates were observed to grow into longer fibrils (Figure 3a, upper two panels, and Videos S1, S2), while the majority of the existing PrP seeds showed no detectable change in length. Consistent with the observation of an increase in aggregate length, the ThT intensity of individual aggregates increased with length both in soluble and insoluble seeding cases (Figure S4a,b). The slower increase in the average length for insoluble seeds compared to soluble seeds could be due to structural difference of the seeds resulting in different growth rates (Figure S4c).

DOI: 10.1021/jacs.8b08311
J. Am. Chem. Soc. 2018, 140, 14789−14798

Table 1. Kinetic Parameters for PrP and αS Aggregation in Solution[a]

protein	k_e (M^{-1} s^{-1})	k_f (s^{-1})	$k_e k_f$ (M^{-1} s^{-2})	m (nM)	t_2	PK-sen to PK-res conversion half-time
PrP	~10^4 [b]	~10^{-6} [b]	0.06 ± 0.03	60 (PM)	2.2 ± 1.1 h	<0.25 h
				15 (EC)	4.4 ± 2.2 h	
αS	43 ± 7	1.6 ± 0.2 × 10^{-10}	6.9 ± 1.4 × 10^{-9}	2000 (SN)	48 ± 2 day	39.5 ± 7.3 h

[a] k_e elongation rate constant; k_f fragmentation rate constant; m local concentration of monomers in the cells; t_2 doubling time required for a single protein aggregate to replicate into two aggregates during aggregation. PM: plasma membrane; EC: endosomal compartments; SN: synapse. The errors represent uncertainties of the fitting parameters given the dataset. [b] Estimate is within the same order of magnitude.

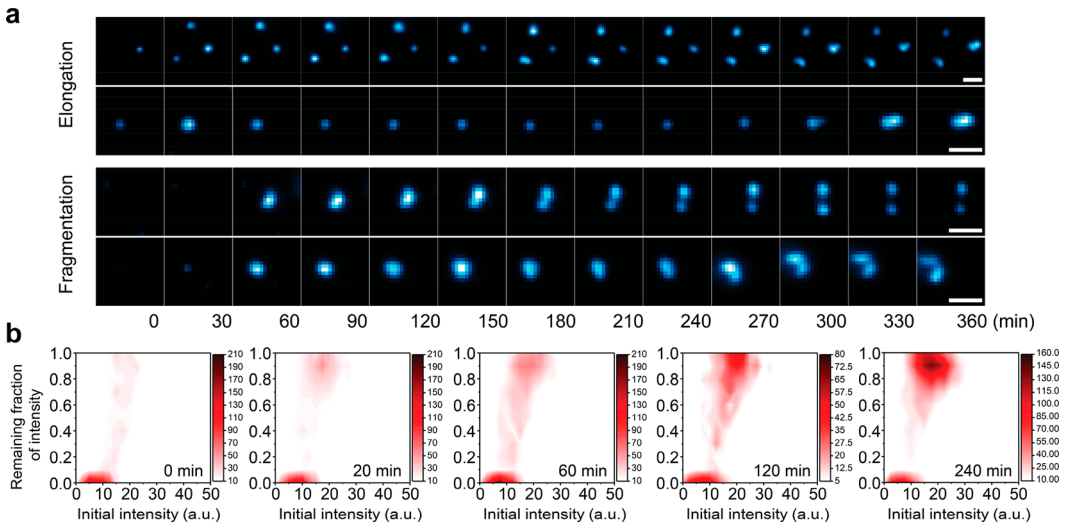

Figure 3. Direct measurement of PrP fibril elongation and fragmentation. (a) The representative examples of PrP elongation (upper panel, see Videos S1, S2) and PrP fragmentation (lower panel, see Videos S3, S4) were recorded over a 6 h period during surface-seeded aggregation with soluble seeds in 50 mM sodium phosphate (pH 7.0) at 37 °C. Individual particles were tracked over time by imaging with fixed fields of view every 5 min. The scale bars represent 2 μm. (b) Proteinase K (PK) resistance of PrP aggregates during surface-seeded aggregation. PK was added at different times to the glass surface that contained the PrP aggregates and the slide chamber sealed to prevent fluid evaporation. The change in ThT intensity of individual particles was followed by continual imaging with fixed fields of view at 37 °C incubation. PK resistance was calculated as the fraction of the ThT intensity after 1 h proteolytic digestion compared to that seen at the start of the experiment.

Table 2. Kinetic Parameters for Surface-Seeded PrP[a]

seed type	k_e (M^{-1} s^{-1})	k_f (s^{-1})[b]	$k_e k_f$ (M^{-1} s^{-2})[b]	PK-sen to PK-res conversion half-time
soluble seed	3.39 ± 0.04 × 10^4	≥5 × 10^{-9}	≥0.00017	0.25 h
insoluble seed	1 × 10^4	≥1.6 × 10^{-8}	≥0.00016	

[a] k_e elongation rate constant; k_f fragmentation rate constant. The errors represent uncertainties of the fitting parameters given the dataset. [b] Measured as the slowest value.

Strikingly, fragmentation events of PrP fibrils that involved one fibrillar assembly breaking into two or more smaller-sized fragments were directly observed. These fragments were shown to be capable of growing into longer fibrils at later times (Figure 3a, lower two panels, and Videos S3, S4). The fragmentation events account for only 0.4% (soluble) and 0.9% (insoluble) of the total events recorded for each type of seed. In addition, a fraction of the fragmented PrP species disappeared during the aggregation reaction, which suggested that these small-sized assemblies were not detected by ThT. This is in agreement with our finding from solution-seeded experiments (Figure 2a,b) and TEM imaging (Figure S3) that PrP aggregates can fragment into ThT-inactive species. Centrifugation experiments demonstrated that fluorescence imaging with ThT was able to detect PrP aggregates of 12-mers or larger (Figure S5), which suggested the ThT-inactive species were smaller in size.

Although a similar real-time imaging approach has previously been used to follow fibril formation of β2-microglobulin[31] and Aβ,[32] the molecular mechanism was not discussed or quantified despite the importance in understanding prion propagation. To measure the kinetic rate constants for PrP aggregation on a surface, we fitted the average rate of increase of fibril length as a function of time (Figure S4c). The fragmentation rate constants were estimated as $k_{f\,(\text{soluble})} \geq 5 \times 10^{-9}$ s^{-1} and $k_{f\,(\text{insoluble})} \geq 1.6 \times 10^{-8}$ s^{-1} for soluble and insoluble seeding, respectively. In contrast, the elongation rate constants were estimated as $k_{e\,(\text{soluble})} = 3.39 \times 10^4$ M^{-1} s^{-1} and $k_{e\,(\text{insoluble})} = 1 \times 10^4$ M^{-1} s^{-1} (Table 2). The different rate constants for the soluble and insoluble seed is likely to result from the different structures. It should be noted that we used " ≥ " for k_f values because of potential underestimation, as there may be fragmentation events that were unable to be detected as shown in Figure S3. We also observed that the product of k_e and k_f for the soluble seed is ≥0.00017 M^{-1} s^{-2} in surface-seeded reaction, which is slower than 0.06 M^{-1} s^{-2} in bulk solution-seeded reaction by 2 orders of magnitude. This may reflect differences between aggregation in solution and on the surface, but may also be due to the under estimation of k_f obtained in the surface-seeded

DOI: 10.1021/jacs.8b08311
J. Am. Chem. Soc. 2018, 140, 14789−14798

experiments, resulting in a lower $k_e k_f$. However, the slower surface-seeded reaction allowed us to directly observe fragmentation and also measure changes in PK resistance.

PrP Aggregates Undergo Structural Conversion from PK-Sensitive to PK-Resistant Conformation. To assess the susceptibility of PrP aggregates to Proteinase K (PK) digestion, we carried out proteolytic digestion at single-aggregate level during surface-seeded aggregation with soluble seeds. This was achieved by the addition of PK at defined time points during the seeded aggregation reaction and subsequent measurement of the decrease of ThT intensity of individual PrP assemblies induced by proteolytic digestion. Initially, the soluble seeds were predominantly PK-sensitive (PK-sen), as very few PrP assemblies remained detectable after 1 h digestion with PK. With increasing time, more aggregates maintained high ThT intensity after PK digestion (Figure 3b). This suggested that accumulation of PK-resistant species (PK-res) occurred with time and that a structural conversion occurred during PrP aggregation. Furthermore, compared to PK-sen species, the PK-res species possessed higher initial ThT intensity before PK digestion, which indicated these assemblies were also larger in size since the length-intensity relationship was demonstrated to be linear (Figure S6).

Next, we quantified the fractions of the PK-sen and PK-res species by fitting with 2D Gaussian functions and hence acquired the kinetic profiles shown in Figure 4. The number of

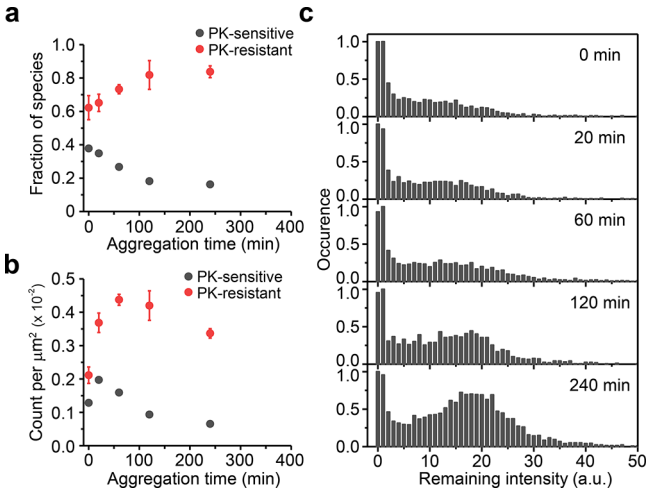

Figure 4. Structural conversion of PrP aggregates. Temporal change in (a) the fraction and (b) the number of PK-sen and PK-res species of surface-seeded PrP aggregates using soluble seeds. The data set from Figure 2b were globally fitted to 2D Gaussian functions to obtain the fraction of PK-sen and PK-res populations. (c) Intensity distributions after PK-digestion for surface-seeded PrP aggregates at different time points. The error bars represent standard deviations from three independent experiments.

PK-res aggregates showed a fast increase and reached a maximum level after 1 h aggregation. This suggested a fast PK-sen → PK-res conversion reaction occurred with a half-time of ~0.25 h (Table 1). As the replication rate of PrP was slower on the surface due to lower $k_e k_f$, this conversion rate on the surface was likely to be slower than that in bulk solution, which is expected to be <0.25 h.

Fragmentation of PrP Fibrils Follows a Length-Dependent Mechanism and Is Accompanied by Loss of PK Resistance. The fragmentation rate constant, k_f, in our kinetic model was calculated per monomer in an aggregated assembly. A fibril may potentially fragment at random positions along its length, and hence the rate of fragmentation would be expected to increase with fibril length (i.e., a 1000-mer fibril is expected to have fragmentation rate higher than the k_f value by 1000-fold). Since very few studies have demonstrated the molecular details of fibril fragmentation, we measured this process on the coverslip surface to probe the length dependence. Fragmentation of individual PrP fibrils was followed continually over 72 h in fixed fields of view, and the decrease in the average fibril length (i.e., fragmentation) was measured. A higher fragmentation rate was revealed with increasing fibril length (Figure 5a and S7). The kinetic profiles were in good agreement with the PrP fibril fragmentation fits based on our kinetic model, which suggested that the fragmentation rate of a fibril is proportional to its fibril length, and that our previous assumption was justified.

Next, we examined the susceptibility of fragmented PrP fibrils to PK digestion at defined time points (Figure 5c). Surprisingly, PrP fibrils rapidly lost resistance to PK despite our observation that the number of PK-sen aggregates remained approximately constant (Figure 5b). The PK-res species that have peak intensity at 10 au became PK-sen, while the less intense PK-sen species peaked at 5 au disappeared, presumably due to fragmentation into smaller species that were not ThT-active. This suggested that the PK-sen aggregates at later times are more likely to be generated from the initially PK-res fibrils by a structural conversion.

Aggregation of α-Synuclein Is Associated with Slower Fragmentation Rate than PrP. Protein inclusions of α-synuclein (αS) are the neuropathological hallmark of Parkinson's disease (PD) and related synucleinopathies including dementia with Lewy bodies (DLB) and multiple system atrophy (MSA). αS has been reported to exhibit transcellular spread by a prion-like mechanism.[33−35] Hence, we investigated the propagation characteristics of human αS in comparison with those associated with PrP replication. Seeded or unseeded human αS aggregation reactions were performed in bulk solution under native conditions to determine the change in aggregate length with respect to time (Figure 1, left and Figure 6a). In unseeded αS aggregation, we observed an initial increase in the average aggregate length, followed by a slow decrease at later times over a long period of several weeks. The decrease of aggregate length was shown not to be due to proteolysis (Figure S8), which suggested it is likely to result from fragmentation of αS fibrils. To extract the kinetic parameters of αS aggregation, we fitted the kinetic profiles and estimated k_e and k_f for αS. With these values we calculated the product of k_e and k_f of 6.9×10^{-9} M^{-1} s^{-2}, which is lower than the equivalent value for PrP in solution by a factor of 10^7 (Table 1). Given the αS concentration of neuron synapses in the mouse brain was estimated to be 2 μM,[36] the derived doubling time t_2 for αS is 48 days. This suggested that the time for αS to replicate was approximately 1000-fold longer than that of PrP replication. This calculation provides a quantitative approach to estimate to what extent αS is "prion-like" through the kinetic parameters measured.

We also analyzed the PK resistance for αS assemblies at defined time points during its aggregation (Figure 6b). It was found that αS aggregates were initially PK-sensitive and subsequently acquired PK resistance as the assemblies grew in length into longer fibrils. Likewise, the fractions of the PK-sen and PK-res species of αS were quantified by fitting with 2D

DOI: 10.1021/jacs.8b08311
J. Am. Chem. Soc. 2018, 140, 14789−14798

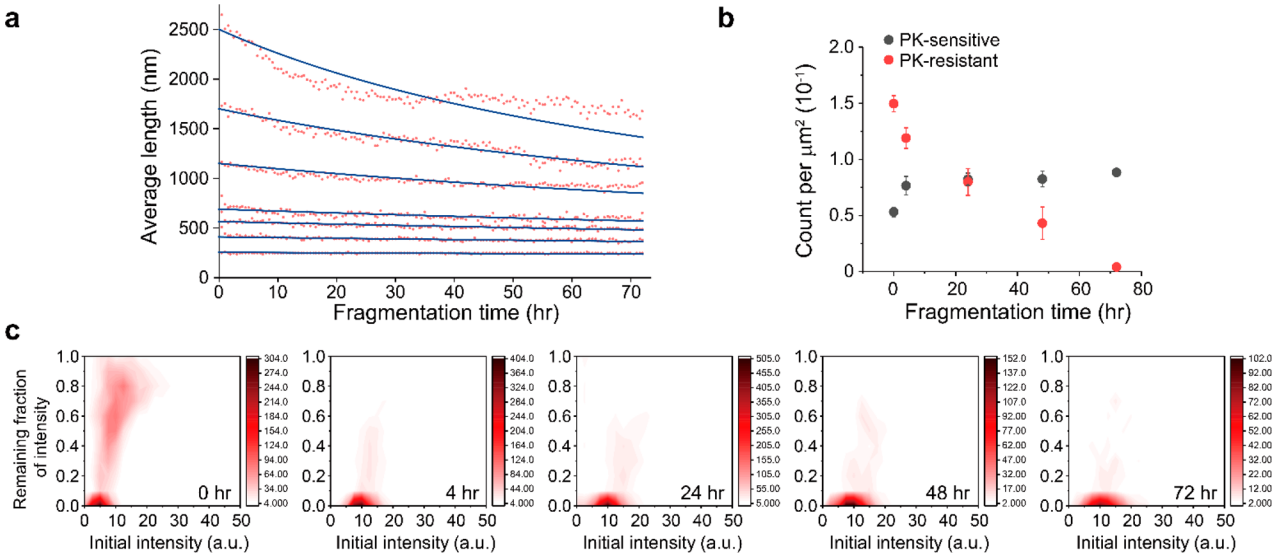

Figure 5. PrP fibril fragmentation. (a) Time-dependent change in average PrP fibril length, for a range of initial lengths. The data shown correspond to the average of three independent experiments. (b) Proteinase K (PK) resistance of PrP aggregates during surface-seeded aggregation. PK was added at different times to the glass surface that contained the PrP aggregates, and the slide chamber was sealed to prevent fluid evaporation. The change in ThT intensity of individual particles was followed by continual imaging with fixed fields of view at 37 °C incubation. PK resistance was calculated as the fraction of the ThT intensity after 1 h proteolytic digestion compared to that seen at the start of the experiment. The error bars represent standard deviations from three independent experiments. (c) Temporal change in the fraction and the number of PK-sen and PK-res species of PrP fragments as a function of time. The data set from (b) was globally fitted to 2D-Gaussian functions to obtain the fraction of PK-sen and PK-res populations as a function of time.

Gaussian functions and hence kinetic profiles acquired. The fraction of PK-res aggregates increased rapidly and reached a plateau after 2 days (Figure 7a), while the number of these assemblies increased continuously over time (Figure 7b). The conversion of αS aggregates from PK-sen to PK-res forms was determined to have a half time of ∼39.5 h, which is in good agreement with our previous FRET measurements.[20] In comparison with the half-time for PrP conversion, αS aggregates required >100 fold more time for structural conversion (Table 1) despite the fact that the aggregation would appear to occur by a similar mechanism.

Estimation for the Spreading Time of PrP and αS in the Brain. It has been demonstrated that the growth rate of different strains in yeast prion Sup35 can be predicted by a simple model which takes into account monomer concentration, the rate of cell division, and the elongation and fragmentation rates of different strains.[14] With a similar model, we previously estimated the spreading of tau replication in the brain using experimentally measured kinetic parameters, showing that tau accumulation in the brain is likely to follow an exponential behavior resulting from fragmentation.[23] Here, we tested this spreading model with PrP and αS using the kinetic parameters that we acquired in Table 1.

Sustainable spreading of protein aggregates in the cells involves both effective seeding and amplification, as discussed in our previous study.[16] In this scenario, a single PrP aggregate in a cell can grow and then fragment into two smaller assemblies. The two assemblies thus act as new templates and are able to enter neighboring cells in order to support sustained spreading. Therefore, the accumulated number of PrP aggregates is exponential and given by

$$f(n) = f_0 \cdot 2^n \tag{2}$$

where f_0 is the initial number of aggregates and n is the round of doubling required to reach a final number of aggregates $f(n)$.

On the basis of the rounds of doubling (n) and doubling time (t_2) in eq 1, one can calculate the hypothetical spreading time ($T_{spreading}$) required to obtain a certain number of aggregates in the brain:

$$T_{spreading} = n \cdot t_2 \tag{3}$$

Next, we asked how fast PrP aggregates would hypothetically spread in the mouse brain based on our findings when a single aggregate is effectively seeded on the plasma membrane. According to the eq 2 and 3, we plotted the accumulation of PrP aggregates as a function of time and then calculated $T_{spreading}$ (Figure S9a).

In a typical mouse brain, there are approximately 70 million neurons. To obtain one PrP aggregate in every neuron on average, it would take 2.4 days for a wild-type $Prnp^{+/+}$ mouse through exponential replication. For a $Prnp^{+/-}$ mouse (∼0.5× PrP expression level) and a tg20 mouse (∼8× PrP expression level), it would take 3.4 and 0.8 days, respectively (Table S1). As we have discussed previously, PrP levels at different conversion sites only have a mild effect upon t_2, and hence do not alter $T_{spreading}$ to a great extent. The hypothetical calculation of PrP spreading agrees with the experimental incubation periods observed in mice models within 2 orders of magnitude. The experimentally determined incubation periods are 137 ± 1.5, 258 ± 24, and 59.5 ± 2 days for $Prnp^{+/+}$, $Prnp^{+/-}$, and tg20 mice, respectively.[37] Importantly, the relative ratios of $T_{spreading}$ between the three mouse strains ($Prnp^{+/-}$, $Prnp^{+/+}$, tg20) predicted from our model are very similar to those from animal experiments.

With the same rationale, we repeated the above calculations using the rate constants obtained for αS (Figure S9a). As we obtained a t_2 of 48 days for αS in the mouse brain, $T_{spreading}$ was predicted to be ∼3.4 years in order to spread through an entire mouse brain (Table S1). This is in surprisingly good agreement with the experimental results of 15 months

DOI: 10.1021/jacs.8b08311
J. Am. Chem. Soc. 2018, 140, 14789−14798

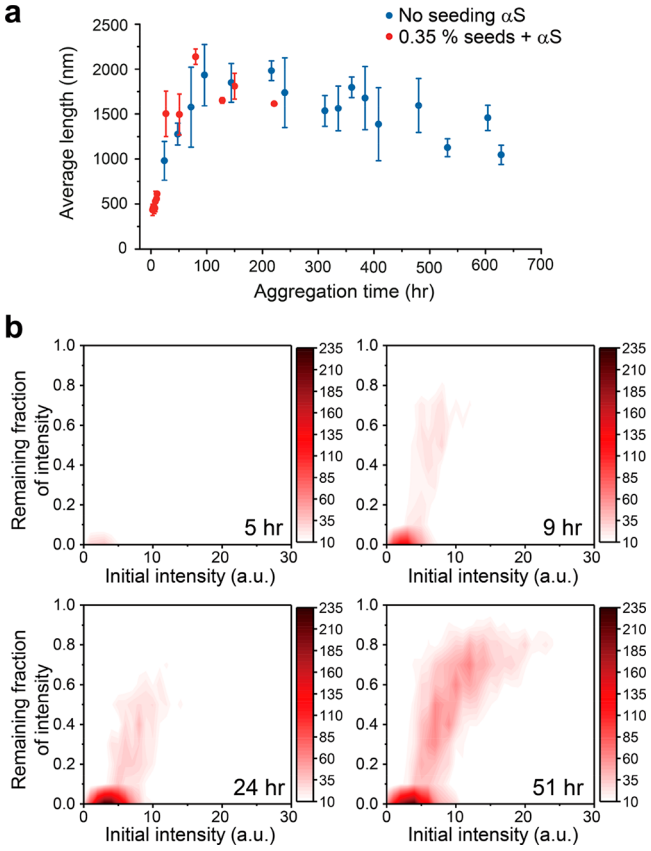

Figure 6. Kinetics of αS aggregation. (a) Kinetics of seeded- and nonseeded solution-seeded α-synuclein aggregation in 50 mM sodium phosphate buffer (pH 7.0). Reaction kinetics were measured by taking aliquots at various time points from aggregation reaction mix that was incubated at 37 °C with shaking at 200 rpm. The kinetic data obtained were used to estimate the fragmentation and elongation rate constants k_e and k_f, respectively. The product of rate constants $k_e k_f$ is 6.9 ± 1.4 × 10^{-9} M^{-1} s^{-2}. The error bars represent standard deviations from three independent experiments. (b) Proteinase K (PK) resistance of αS aggregates. αS aggregates induced by sonicated fibrils were incubated in a 1.5 mL centrifuge tube. At various time points, aliquots were removed from the reaction mix and adsorbed onto a glass coverslip. PK was added at different times to the glass coverslip and slide chamber sealed to prevent fluid evaporation. The change in ThT intensity of individual particles was followed by continual imaging with the fixed fields of view at 37 °C incubation. PK resistance was calculated as the fraction of the ThT intensity after 1 h proteolytic digestion compared to that seen at the start of the experiment.

duration, which is required for 90% of the WT mouse brain cells to acquire αS inclusions after intracerebral injection of the human αS seed.[38] Despite having significantly slower elongation and fragmentation rates than PrP, our model suggests that αS follows a similar prion-like mechanism of spreading in vivo.

DISCUSSION

We have directly observed the elongation and fragmentation of murine PrP. Although fragmentation has been proposed to be an important factor for sustained prion replication, this is the first time to our knowledge that fragmentation has been directly observed. Our results show that amplification of the number of PrP aggregates occurs by an elongation/fragmentation mechanism, and PrP fibrils fragment with a

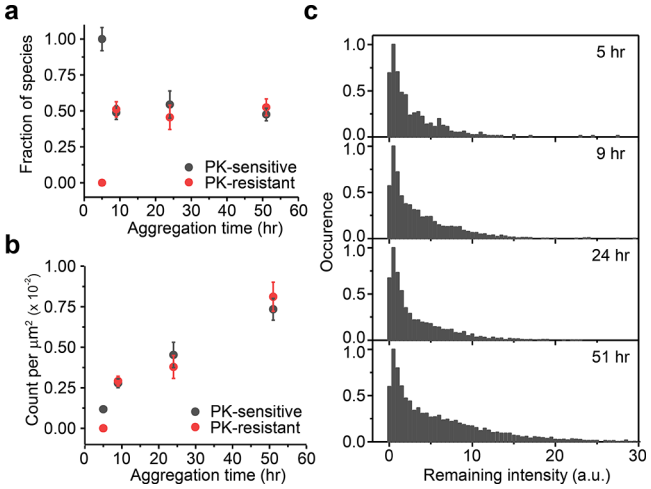

Figure 7. Structural conversion of αS aggregates. Temporal change in (a) the fraction and (b) the number of PK-sen and PK-res species of αS aggregates as a function of time. The data set from Figure 6b were globally fitted to 2D Gaussian functions to obtain the fraction of PK-sen and PK-res populations as a function of time. (c) Intensity distributions after PK-digestion at different time points.

substantially higher rate compared with αS. Surface-seeded experiments reveal fibril fragmentation rate is proportional to fibril length. This suggests that larger-sized fibrils are more likely to break and thus produce new templates for further replication.

We also observed that during the aggregation process PrP undergoes structural conversion from a PK-sen to PK-res conformer. This is consistent with previous studies in mice where PK-res and PK-sen PrP species accumulated during prion propagation.[7,37] However, in our experiments reported here we observed that during fragmentation PrP fibrils rapidly lose PK resistance, possibly due to destabilization of the fibrillar structure. Our finding would argue that reversion of PK resistance occurs when the fibrillar structure becomes fragile. Despite the fragility of fibril fragments, they are able to form new fibrils as directly observed on the surface and regain resistance to PK. Our observations partly explain the production of disease-related PK-sen species observed in vivo.[37,39−42] Fragmentation of large PrP fibrils at later times is likely to produce more PK-sen segments and thus exceed the formation of new PK-resistant fibrils, which is consistent with the finding that the PK-sen species constitutes the majority of total PrP level at the late stage of prion propagation in mice.[37]

Through determination of the rate constants, k_e and k_f, we were able to calculate the t_2 for PrP replication at the physiological protein concentration in cells, and hence establish a simple spreading model based on these kinetic measurements. PrP replication shows unusually fast elongation/fragmentation and results in t_2 = 2.2 h (Table 1), leading to an estimate of the time to spread throughout the mouse brain as a few days. The discrepancy between our prediction and in vivo experimental data can be explained by several cellular mechanisms that we did not consider in our spreading model. These include organelle confinement and active clearance and the degradation of misfolded proteins.[43] The presence of the lipid membrane has been shown to restrict the motion of Aβ oligomers on the lipid membrane[44], so since PrP is a GPI-anchored protein predominantly found within lipid rafts on the plasma membrane,[45] it is likely that the rate of PrP

DOI: 10.1021/jacs.8b08311
J. Am. Chem. Soc. 2018, 140, 14789−14798

spreading in vivo may be also altered due to clustering and slower diffusion on the membrane. PrP glycosylation has also been demonstrated to decrease PrP^{Sc} amplification in PMCA by 10−10 000 fold.[46,47] Furthermore, specific cofactors would appear to be necessary for faithful prion propagation in a strain-specific manner,[48] which appears to be a general phenomenon that is not restricted to mammalian hosts.[49] The effect of the above mechanisms on the rate of spreading is not understood, and so it is not possible to include these factors in our current kinetic model. However, these factors are likely to decrease the rate of PrP spreading in vivo, by either reducing the replication efficiency or increasing t_2. Our data also show that αS replication is similar to PrP, occurring through an elongation−fragmentation mechanism at much slower rates. This provides a quantitative approach to estimate the prion-like property of αS based on its aggregation kinetics. On the basis of the observation of longer t_2, we predict that αS aggregates would spend significant time in cells without degradation as has recently been observed.[50]

Our kinetic approach may also explain the differences in amplification rate of different prion strains. The diversity of prion strains represent different conformational states of PrP^{Sc} within the same genotype that directly influence host range and clinicopathological features of prion diseases in the affected host.[51] On the basis of eq 1, if a given prion strain (F) has faster t_2 (i.e., higher k_e or k_f value) than a slow strain (S), the number of prion strain F would be substantially greater than that of prion strain S after multiple rounds of doubling (see Supporting Information for calculations). For example, if prion strain F has a t_2 10% lower than prion strain S (i.e., approximately 20% higher in $k_e k_f$), after 26 rounds of doubling (the number of doubling rounds needed for one aggregate of strain F to replicate so there is an aggregate in every neuron in a mouse brain, see Table S1) , a 5-fold excess of F-strain aggregates will be produced. Therefore, small differences in kinetic rate constants or replication efficiency would appear to be able to contribute to an explanation of the diversity in prion strains.

In summary, we have directly observed spontaneous fibril fragmentation and elongation for PrP and αS in vitro and hence measured their fragmentation and elongation rate constants. During the aggregation of PrP and αS, these proteins undergo structural conversion from PK-sen to PK-res conformers. Furthermore, fragmentation of the aggregated forms of these proteins follows a length-dependent mechanism leading to the formation of PK-sen fragments. The measurement of the kinetic parameters involved in these processes has allowed us to estimate the rate of spread of prion and prion-like aggregates in the brain. Our model explains some of the key features of prion diseases and makes quantitative predictions that can be tested experimentally about the spreading of PrP and other prion-like proteins such as αS.

■ ASSOCIATED CONTENT

Supporting Information

The Supporting Information is available free of charge on the ACS Publications website at DOI: 10.1021/jacs.8b08311.

Additional experimental procedures, supplementary figures, tables, and video descriptions (PDF)

Video S1 (AVI)

Video S2 (AVI)

Video S3 (AVI)

Video S4 (AVI)

■ AUTHOR INFORMATION

Corresponding Author

*dk10012@cam.ac.uk

ORCID

Jason C. Sang: 0000-0002-8567-5415

Georg Meisl: 0000-0002-6562-7715

Tuomas P. J. Knowles: 0000-0002-7879-0140

Notes

The authors declare no competing financial interest.

■ ACKNOWLEDGMENTS

We thank Swapan Preet for expression and purification of α-synuclein and Dr. J. N. Skepper in the Cambridge Advanced Imaging Centre for assistance with TEM imaging. We are grateful to Dr. Michel Goedert for helpful suggestions in the spreading model. J. C. S. is supported by a Cambridge Trust Scholarship and a Ministry of Education Technologies Incubation Scholarship, Republic of China (Taiwan). L. H. was supported by the Tsinghua University Initiative Scientific Research Program (Grants 20151080424) and the program of China Scholarships Council (CSC). A. M. T was supported in part by an MRC (NC3Rs) Project (Grant NC/K000462/1). G. M. and T. P. J. K. wish to acknowledge support from Sidney Sussex College Cambridge and the ERC grant PhysProt (337969). A. P. acknowledges funding from EPSRC (Grant EP/L027631/1). D. K. acknowledges funding from the Royal society and an ERC Advanced Grant (669237).

■ REFERENCES

(1) Prusiner, S. B. Novel Proteinaceous Infectious Particles Cause Scrapie. *Science* **1982**, *216* (4542), 136−144.

(2) Nazor, K. E.; Kuhn, F.; Seward, T.; Green, M.; Zwald, D.; Pürro, M.; Schmid, J.; Biffiger, K.; Power, A. M.; Oesch, B.; Raeber, A. J.; Telling, G. C. Immunodetection of Disease-Associated Mutant PrP, Which Accelerates Disease in GSS Transgenic Mice. *EMBO J.* **2005**, *24* (13), 2472−2480.

(3) Hsiao, K. K.; Groth, D.; Scott, M.; Yang, S. L.; Serban, H.; Rapp, D.; Foster, D.; Torchia, M.; Dearmond, S. J.; Prusiner, S. B. Serial Transmission in Rodents of Neurodegeneration from Transgenic Mice Expressing Mutant Prion Protein. *Proc. Natl. Acad. Sci. U. S. A.* **1994**, *91* (19), 9126−9130.

(4) Hsiao, K. K.; Scott, M.; Foster, D.; Groth, D. F.; DeArmond, S. J.; Prusiner, S. B. Spontaneous Neurodegeneration in Transgenic Mice with Mutant Prion Protein. *Science* **1990**, *250* (4987), 1587−1590.

(5) Zhang, Z.; Zhang, Y.; Wang, F.; Wang, X.; Xu, Y.; Yang, H.; Yu, G.; Yuan, C.; Ma, J. De Novo Generation of Infectious Prions with Bacterially Expressed Recombinant Prion Protein. *FASEB J.* **2013**, *27* (12), 4768−4775.

(6) Wang, F.; Wang, X.; Yuan, C.-G. C.-G.; Ma, J. Generating a Prion with Bacterially Expressed Recombinant Prion Protein. *Science* **2010**, *327* (5969), 1132−1135.

(7) Collinge, J. Mammalian Prions and Their Wider Relevance in Neurodegenerative Diseases. *Nature* **2016**, *539* (7628), 217−226.

(8) Goedert, M. Alzheimer's and Parkinson's Diseases: The Prion Concept in Relation to Assembled Aβ, Tau, and α-Synuclein. *Science* **2015**, *349* (6248), 1255555.

(9) Luk, K. C.; Kehm, V.; Carroll, J.; Zhang, B.; O'Brien, P.; Trojanowski, J. Q.; Lee, V. M.-Y. Pathological α-Synuclein Transmission Initiates Parkinson-like Neurodegeneration in Nontransgenic Mice. *Science* **2012**, *338* (6109), 949−953.

DOI: 10.1021/jacs.8b08311
J. Am. Chem. Soc. 2018, 140, 14789−14798

(10) Jarrett, J. T.; Lansbury, P. T. Seeding "One-Dimensional Crystallization" of Amyloid: A Pathogenic Mechanism in Alzheimer's Disease and Scrapie? *Cell* **1993**, *73* (6), 1055−1058.
(11) Collins, S. R.; Douglass, A.; Vale, R. D.; Weissman, J. S. Mechanism of Prion Propagation: Amyloid Growth Occurs by Monomer Addition. *PLoS Biol.* **2004**, *2* (10), e321.
(12) Knowles, T. P. J.; Waudby, C. a; Devlin, G. L.; Cohen, S. I. a; Aguzzi, A.; Vendruscolo, M.; Terentjev, E. M.; Welland, M. E.; Dobson, C. M. An Analytical Solution to the Kinetics of Breakable Filament Assembly. *Science* **2009**, *326* (5959), 1533−1537.
(13) Cohen, S. I. A.; Vendruscolo, M.; Dobson, C. M.; Knowles, T. P. J. From Macroscopic Measurements to Microscopic Mechanisms of Protein Aggregation. *J. Mol. Biol.* **2012**, *421* (2−3), 160−171.
(14) Tanaka, M.; Collins, S. R.; Toyama, B. H.; Weissman, J. S. The Physical Basis of How Prion Conformations Determine Strain Phenotypes. *Nature* **2006**, *442* (7102), 585−589.
(15) Yang, J.; Dear, A. J.; Michaels, T. C. T.; Dobson, C. M.; Knowles, T. P. J.; Wu, S.; Perrett, S. Direct Observation of Oligomerization by Single Molecule Fluorescence Reveals a Multistep Aggregation Mechanism for the Yeast Prion Protein Ure2. *J. Am. Chem. Soc.* **2018**, *140* (7), 2493−2503.
(16) Iljina, M.; Garcia, G. A.; Horrocks, M. H.; Tosatto, L.; Choi, M. L.; Ganzinger, K. A.; Abramov, A. Y.; Gandhi, S.; Wood, N. W.; Cremades, N.; Dobson, C. M.; Knowles, T. P. J.; Klenerman, D. Kinetic Model of the Aggregation of Alpha-Synuclein Provides Insights into Prion-like Spreading. *Proc. Natl. Acad. Sci. U. S. A.* **2016**, *113* (9), E1206−15.
(17) Qi, X.; Moore, R. A.; Mcguirl, M. A. Dissociation of Recombinant Prion Protein Fibrils into Short Protofilaments: Implications for the Endocytic Pathway and Involvement of the N-Terminal Domain. *Biochemistry* **2012**, *51* (22), 4600−4608.
(18) Horrocks, M. H.; Lee, S. F.; Gandhi, S.; Magdalinou, N. K.; Chen, S. W.; Devine, M. J.; Tosatto, L.; Kjaergaard, M.; Beckwith, J. S.; Zetterberg, H.; Iljina, M.; Cremades, N.; Dobson, C. M.; Wood, N. W.; Klenerman, D. Single-Molecule Imaging of Individual Amyloid Protein Aggregates in Human Biofluids. *ACS Chem. Neurosci.* **2016**, *7* (3), 399−406.
(19) Orte, A.; Birkett, N. R.; Clarke, R. W.; Devlin, G. L.; Dobson, C. M.; Klenerman, D. Direct Characterization of Amyloidogenic Oligomers by Single-Molecule Fluorescence. *Proc. Natl. Acad. Sci. U. S. A.* **2008**, *105* (38), 14424−14429.
(20) Cremades, N.; Cohen, S. I. A.; Deas, E.; Abramov, A. Y.; Chen, A. Y.; Orte, A.; Sandal, M.; Clarke, R. W.; Dunne, P.; Aprile, F. A.; Bertoncini, C. W.; Wood, N. W.; Knowles, T. P. J.; Dobson, C. M.; Klenerman, D. Direct Observation of the Interconversion of Normal and Toxic Forms of α-Synuclein. *Cell* **2012**, *149* (5), 1048−1059.
(21) Ganzinger, K. A.; Narayan, P.; Qamar, S. S.; Weimann, L.; Ranasinghe, R. T.; Aguzzi, A.; Dobson, C. M.; McColl, J.; St George-Hyslop, P.; Klenerman, D. Single-Molecule Imaging Reveals That Small Amyloid-B1−42 Oligomers Interact with the Cellular Prion Protein (PrP(C)). *ChemBioChem* **2014**, *15* (17), 2515−2521.
(22) Shammas, S. L.; Garcia, G. A.; Kumar, S.; Kjaergaard, M.; Horrocks, M. H.; Shivji, N.; Mandelkow, E.; Knowles, T. P. J.; Mandelkow, E.; Klenerman, D. A Mechanistic Model of Tau Amyloid Aggregation Based on Direct Observation of Oligomers. *Nat. Commun.* **2015**, *6*, 7025.
(23) Kundel, F.; Hong, L.; Falcon, B.; McEwan, W. A.; Michaels, T. C. T.; Meisl, G.; Esteras, N.; Abramov, A. Y.; Knowles, T. J. P.; Goedert, M.; Klenerman, D. Measurement of Tau Filament Fragmentation Provides Insights into Prion-like Spreading. *ACS Chem. Neurosci.* **2018**, *9* (6), 1276−1282.
(24) Dutta, A.; Chen, S.; Surewicz, W. K. The Effect of B2-A2 Loop Mutation on Amyloidogenic Properties of the Prion Protein. *FEBS Lett.* **2013**, *587* (18), 2918−2923.
(25) Kang, H.-E.; Mo, Y.; Abd Rahim, R.; Lee, H.-M.; Ryou, C. Prion Diagnosis: Application of Real-Time Quaking-Induced Conversion. *BioMed Res. Int.* **2017**, *2017*, 5413936.
(26) Meisl, G.; Kirkegaard, J. B.; Arosio, P.; Michaels, T. C. T.; Vendruscolo, M.; Dobson, C. M.; Linse, S.; Knowles, T. P. J. Molecular Mechanisms of Protein Aggregation from Global Fitting of Kinetic Models. *Nat. Protoc.* **2016**, *11* (2), 252−272.
(27) Mironov, A.; Latawiec, D.; Wille, H.; Bouzamondo-Bernstein, E.; Legname, G.; Williamson, R. A.; Burton, D.; DeArmond, S. J.; Prusiner, S. B.; Peters, P. J. Cytosolic Prion Protein in Neurons. *J. Neurosci.* **2003**, *23* (18), 7183−7193.
(28) Godsave, S. F.; Wille, H.; Kujala, P.; Latawiec, D.; DeArmond, S. J.; Serban, A.; Prusiner, S. B.; Peters, P. J. Cryo-Immunogold Electron Microscopy for Prions: Toward Identification of a Conversion Site. *J. Neurosci.* **2008**, *28* (47), 12489−12499.
(29) Goold, R.; Rabbanian, S.; Sutton, L.; Andre, R.; Arora, P.; Moonga, J.; Clarke, A. R.; Schiavo, G.; Jat, P.; Collinge, J.; Tabrizi, S. J. Rapid Cell-Surface Prion Protein Conversion Revealed Using a Novel Cell System. *Nat. Commun.* **2011**, *2*, 281.
(30) Godsave, S. F.; Wille, H.; Pierson, J.; Prusiner, S. B.; Peters, P. J. Plasma Membrane Invaginations Containing Clusters of Full-Length PrPSc Are an Early Form of Prion-Associated Neuropathology in Vivo. *Neurobiol. Aging* **2013**, *34* (6), 1621−1631.
(31) Ban, T.; Hamada, D.; Hasegawa, K.; Naiki, H.; Goto, Y. Direct Observation of Amyloid Fibril Growth Monitored by Thioflavin T Fluorescence. *J. Biol. Chem.* **2003**, *278* (19), 16462−16465.
(32) Ban, T.; Hoshino, M.; Takahashi, S.; Hamada, D.; Hasegawa, K.; Naiki, H.; Goto, Y. Direct Observation of Abeta Amyloid Fibril Growth and Inhibition. *J. Mol. Biol.* **2004**, *344* (3), 757−767.
(33) Chauhan, A.; Jeans, A. F. Is Parkinson's Disease Truly a Prion-like Disorder? An Appraisal of Current Evidence. *Neurol. Res. Int.* **2015**, *2015*, 345285.
(34) Brundin, P.; Li, J.-Y.; Holton, J. L.; Lindvall, O.; Revesz, T. Research in Motion: The Enigma of Parkinson's Disease Pathology Spread. *Nat. Rev. Neurosci.* **2008**, *9* (10), 741−745.
(35) Golde, T. E.; Borchelt, D. R.; Giasson, B. I.; Lewis, J. Thinking Laterally about Neurodegenerative Proteinopathies. *J. Clin. Invest.* **2013**, *123* (5), 1847−1855.
(36) Westphal, C. H.; Chandra, S. S. Monomeric Synucleins Generate Membrane Curvature. *J. Biol. Chem.* **2013**, *288* (3), 1829−1840.
(37) Sandberg, M. K.; Al-Doujaily, H.; Sharps, B.; DeOliveira, M. W.; Schmidt, C.; Richard-Londt, A.; Lyall, S.; Linehan, J. M.; Brandner, S.; Wadsworth, J. D. F.; Clarke, A. R.; Collinge, J. Prion Neuropathology Follows the Accumulation of Alternate Prion Protein Isoforms after Infective Titre Has Peaked. *Nat. Commun.* **2014**, *5* (May), 4347.
(38) Masuda-Suzukake, M.; Nonaka, T.; Hosokawa, M.; Oikawa, T.; Arai, T.; Akiyama, H.; Mann, D. M. A.; Hasegawa, M. Prion-like Spreading of Pathological α-Synuclein in Brain. *Brain* **2013**, *136* (4), 1128−1138.
(39) Colby, D. W.; Wain, R.; Baskakov, I. V.; Legname, G.; Palmer, C. G.; Nguyen, H.-O. B.; Lemus, A.; Cohen, F. E.; DeArmond, S. J.; Prusiner, S. B. Protease-Sensitive Synthetic Prions. *PLoS Pathog.* **2010**, *6* (1), e1000736.
(40) Cronier, S.; Gros, N.; Tattum, M. H.; Jackson, G. S.; Clarke, A. R.; Collinge, J.; Wadsworth, J. D. F. Detection and Characterization of Proteinase K-Sensitive Disease-Related Prion Protein with Thermolysin. *Biochem. J.* **2008**, *416* (2), 297−305.
(41) Tzaban, S.; Friedlander, G.; Schonberger, O.; Horonchik, L.; Yedidia, Y.; Shaked, G.; Gabizon, R.; Taraboulos, A. Protease-Sensitive Scrapie Prion Protein in Aggregates of Heterogeneous Sizes. *Biochemistry* **2002**, *41* (42), 12868−12875.
(42) Safar, J.; Wille, H.; Itri, V.; Groth, D.; Serban, H.; Torchia, M.; Cohen, F. E.; Prusiner, S. B. Eight Prion Strains Have PrP(Sc) Molecules with Different Conformations. *Nat. Med.* **1998**, *4* (10), 1157−1165.
(43) Goold, R.; McKinnon, C.; Tabrizi, S. J. Prion Degradation Pathways: Potential for Therapeutic Intervention. *Mol. Cell. Neurosci.* **2015**, *66* (A), 12−20.
(44) Narayan, P.; Ganzinger, K. A.; McColl, J.; Weimann, L.; Meehan, S.; Qamar, S.; Carver, J. A.; Wilson, M. R.; St George-Hyslop, P.; Dobson, C. M.; Klenerman, D. Single Molecule Characterization of the Interactions between Amyloid-β Peptides

DOI: 10.1021/jacs.8b08311
J. Am. Chem. Soc. 2018, 140, 14789−14798

and the Membranes of Hippocampal Cells. *J. Am. Chem. Soc.* **2013**, *135* (4), 1491−1498.
(45) Naslavsky, N.; Stein, R.; Yanai, A.; Friedlander, G.; Taraboulos, A. Characterization of Detergent-Insoluble Complexes Containing the Cellular Prion Protein and Its Scrapie Isoform. *J. Biol. Chem.* **1997**, *272* (10), 6324−6331.
(46) Katorcha, E.; Makarava, N.; Savtchenko, R.; D'Azzo, A.; Baskakov, I. V. Sialylation of Prion Protein Controls the Rate of Prion Amplification, the Cross-Species Barrier, the Ratio of PrPSc Glycoform and Prion Infectivity. *PLoS Pathog.* **2014**, *10* (9), e1004366.
(47) Katorcha, E.; Makarava, N.; Savtchenko, R.; Baskakov, I. V. Sialylation of the Prion Protein Glycans Controls Prion Replication Rate and Glycoform Ratio. *Sci. Rep.* **2015**, *5*, 16912.
(48) Ma, J. The Role of Cofactors in Prion Propagation and Infectivity. *PLoS Pathog.* **2012**, *8* (4), e1002589.
(49) Thackray, A. M.; Andréoletti, O.; Bujdoso, R. Mammalian Prion Propagation in PrP Transgenic Drosophila. *Brain* **2018**, *141* (9), 2700−2710.
(50) Karpowicz, R. J.; Haney, C. M.; Mihaila, T. S.; Sandler, R. M.; Petersson, E. J.; Lee, V. M.-Y. M. Y. Selective Imaging of Internalized Proteopathic α-Synuclein Seeds in Primary Neurons Reveals Mechanistic Insight into Transmission of Synucleinopathies. *J. Biol. Chem.* **2017**, *292* (32), 13482−13497.
(51) Aguzzi, A.; Heikenwalder, M.; Polymenidou, M. Insights into Prion Strains and Neurotoxicity. *Nat. Rev. Mol. Cell Biol.* **2007**, *8* (7), 552−561.

DOI: 10.1021/jacs.8b08311
J. Am. Chem. Soc. 2018, 140, 14789−14798